fluids

MDPI

Article

Stability or Instability of a Static Liquid Bridge Appearing in Shaped Crystal Growth from Melt via the Pulling-Down Method

Andreea V. Cojocaru [1,†] and Stefan Balint [2,*,†]

[1] Independent Researcher, 300223 Timisoara, Romania; candreeavalentina@gmail.com
[2] Department of Computer Science, West University of Timisoara, 300223 Timisoara, Romania
* Correspondence: stefan.balint@e-uvt.ro
† These authors contributed equally to this work.

Abstract: This study presents sufficient conditions for the stability or instability of the static liquid bridge appearing in crystal growth from the melt of micro-fibers, thin plates, and hollow micro-tubes of predetermined sizes using the pulling-down method. The case in which the contact angle and the growth angle verify the inequality $\alpha_c > \pi/2 - \alpha_g$ is considered. Experimentally, only stable static liquid bridges can be created; unstable static liquid bridges exist just in theory, because in reality they collapse. The results of this study are significant for shaped crystal growth from melted materials, with given macroscopic dimensions, and using specific equipment. This is because the obtained inequalities represent limits for what can and cannot be achieved experimentally.

Keywords: liquid bridge; stability; instability

check for updates

Citation: Cojocaru, A.V.; Balint, S. Stability or Instability of a Static Liquid Bridge Appearing in Shaped Crystal Growth from Melt via the Pulling-Down Method. *Fluids* **2024**, *9*, 176. https://doi.org/10.3390/fluids9080176

Academic Editors: Hua Tan and D. Andrew S. Rees

Received: 19 June 2024
Revised: 26 July 2024
Accepted: 29 July 2024
Published: 31 July 2024

Copyright: © 2024 by the authors. Licensee MDPI, Basel, Switzerland. This article is an open access article distributed under the terms and conditions of the Creative Commons Attribution (CC BY) license (https://creativecommons.org/licenses/by/4.0/).

1. Introduction

Small liquid amounts connecting two solid surfaces, separated by a short distance, are defined as liquid bridges (see Figure 1). These solid surfaces can be surrounded by a gas phase or can be immersed in another liquid immiscible with that of the liquid bridge.

Theoretical and experimental study of these liquid formations has been very extensive during the last century. The shape of liquid bridges of pure liquids is determined by intermolecular forces (liquid–liquid molecular interactions determine surface tension whereas the three-phase contact line is additionally influenced by liquid–solid molecular forces), by gravity, and by external fields such as pressure or electrostatic fields. Although liquid bridges refer to small liquid volumes, they can be found in a range of size scales. Regarding the upper size scale, there is a limit at the physical dimension of about 1 cm. At this size, gravity causes spontaneous collapse of liquid bridges. Even in the absence of gravity (space station experiments or by density matching with the surrounding fluid), there is the so-called Rayleigh stability limit at which some oscillation modes of the bridge become unstable, leading to its disintegration into droplets. For bridges smaller than about 1 mm, the effect of gravity is negligible, and intermolecular forces completely dominate their shape. There is no lower limit to the bridge's physical size beyond that imposed by the molecular nature of the liquid. The situation in the presence of surfactants is much more complex. These molecules not only affect the equilibrium surface tension of the liquid but also bring about a dynamic interfacial behavior of the bridge as they diffuse slowly from the bulk of the bridge towards the gas–liquid interface; see [1].

There are many technological applications where liquid bridges are encountered; see [1–8]. A non-exhaustive list includes processes such as granulation, flotation, and coating. In mechanical engineering, liquid bridges allow control of forces in micro-gripping processes. In geology, liquid bridges determine the properties of moist soil. They are also related to tertiary oil recovery from porous media. A particular recent area of interest refers to self-assembly of particles for which surface tension is the main driving force. New technologies for fabricating micro-electromechanical systems based on liquid bridges have been

proposed. Liquid bridges have been employed as dispensing devices in medical applications. Liquid bridges formed between the tip of the atomic force microscopy probe and the analyzed sample (in humid environments) significantly affect the measurements. Despite the plethora of experimental and theoretical studies on liquid bridges, it is surprising that very few refer to their stability and instability, which factor in shaped single crystal growth from melt material via the edge-defined-film-fed-growth (EFG) and micro-pulling-down (μ-PD) methods. The liquid bridge is a small amount of melt connecting the shaper and the crystal being grown, and in crystal growth this is called the meniscus.

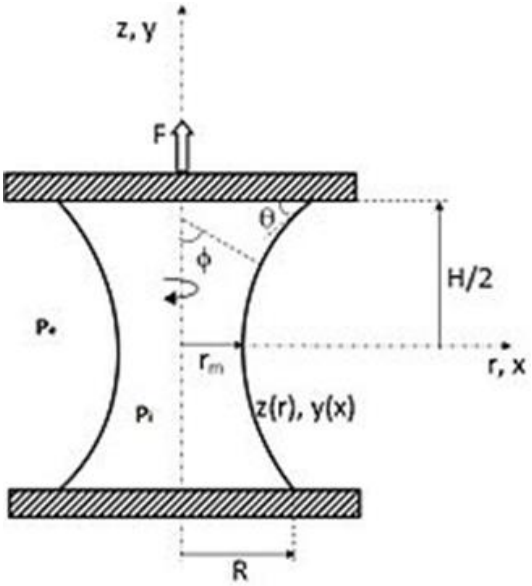


Figure 1. Concave capillary bridge between two planes (schematic representation).

The basic growth methods available for crystal growth are, broadly, growth from the melt, growth from vapor, and growth from solution. *The Springer Handbook of Crystal Growth* [9] presents in 1816 pages the state of the art in crystal growth until the year 2010. In Chapter 40 pg. 1379–1402 of this book, the authors Th. George, St. Balint, and L. Braescu present several mathematical models describing processes that take place in the case of crystal growth from the melt by Bridgman-Stockbarger (BC) and by the edge-defined-film-fed-growth (EFG) method. For the BC method see Figure 2, and for the EFG method see Figures 3–6.

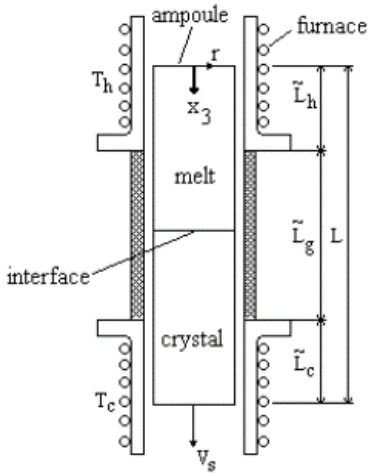


Figure 2. Cylindrical bar BC growth.

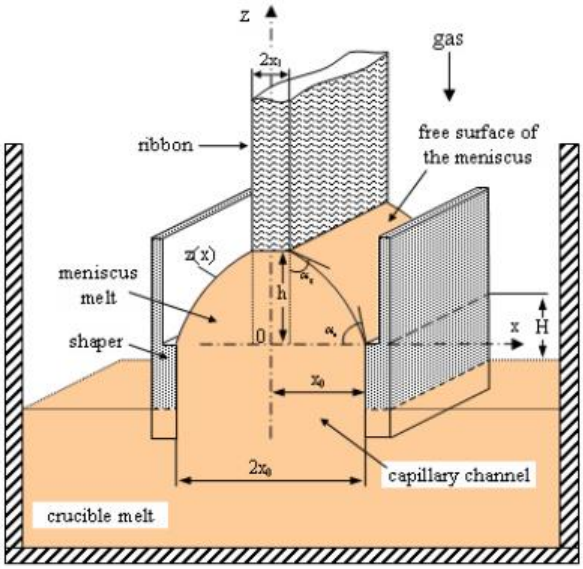


Figure 3. Ribbon EFG growth, case $\alpha_c > \pi/2 - \alpha_g$.

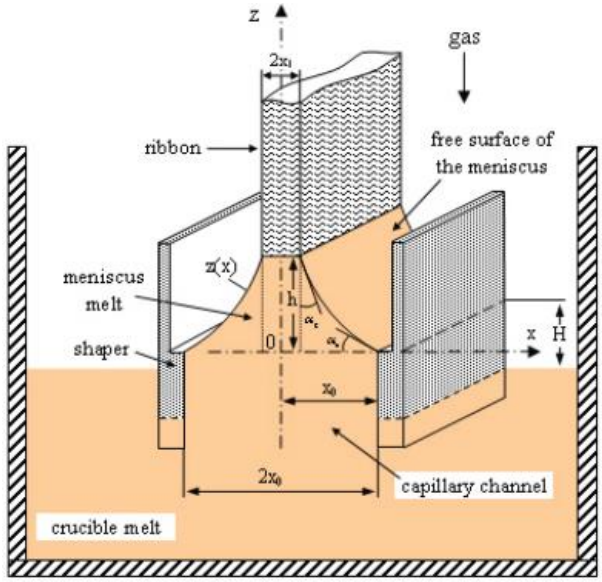


Figure 4. Ribbon EFG growth, case $\alpha_c \leq \pi/2 - \alpha_g$.

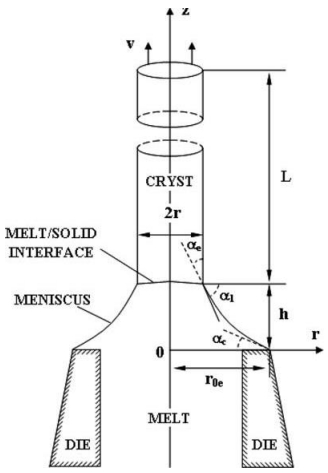


Figure 5. Cylindrical bar EFG growth, case $\alpha_c \leq \pi/2 - \alpha_g$.

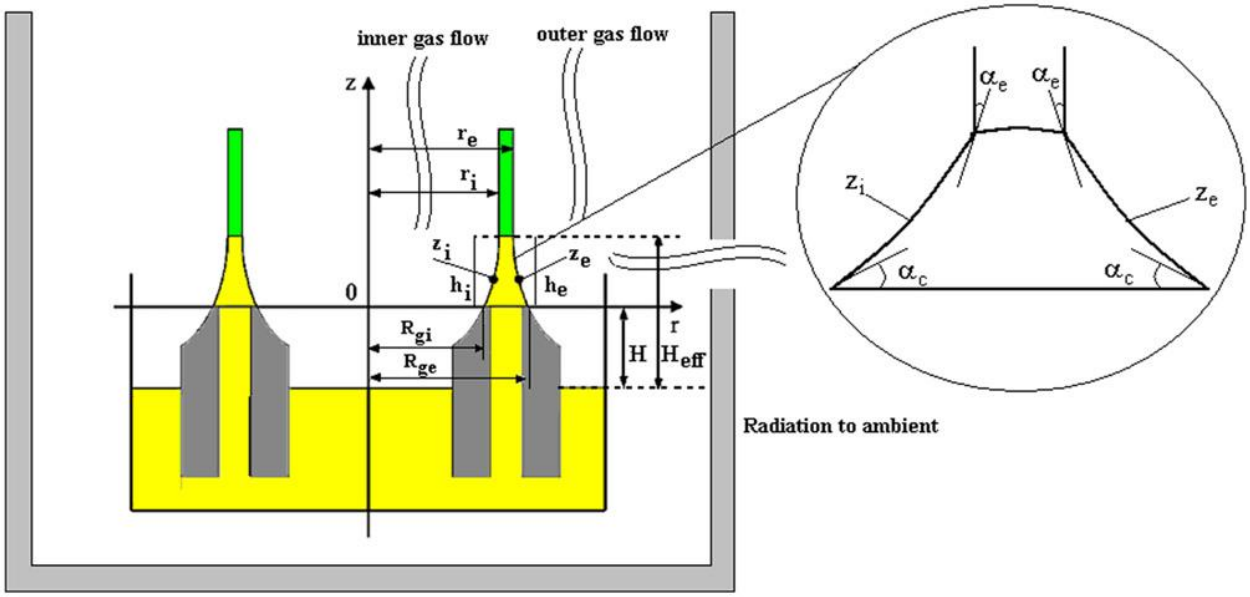


Figure 6. Hollow tube EFG growth, case $\alpha_c \leq \pi/2 - \alpha_g$.

First, a short description is provided of the real processes, which are modeled, along with the equations, boundary conditions, and initial values defining the model. After that, numerical results are provided, obtained from computations in the framework of the model, making a comparison between the computed results and those obtained from other models and with the experimental data. Predictions are made concerning the impurity repartition in the crystal in the framework of each model. The philosophy behind building the mathematical model is to provide a quantitative description of the mechanism by balancing what is wanted with what can be achieved. The quantitative description is made in terms of a certain number of variables (called the model variables) such that the mathematical model is a set of equations concerning these variables. Analysis of the mathematical model leads to results or predictions that can be tested against observations. It is important to realize that all models are idealizations and, hence, are limited in their applicability; experimental verifications can establish the authenticity of the model. In [9] Chapter 40, six models for BS growth (Figure 2) and four models for EFG growth are presented regarding the impurity distribution in the crystal. This is because the quality of the crystal being grown depends to a considerable extent on the homogeneity and distribution of both detrimental and specially added impurities. Variations in the concentrations of impurities along the crystal length and cross section lead to variations in the mechanical, electrical, and optical properties in the mass of the crystal. The impurity repartition in the crystal is determined by the processes that take place in the melt during the growth and mass transfer. Quantitative descriptions of these processes permit the prediction of such repartitioning in the crystal. Consequently, computer modeling of crystal growth processes has often been described as an art as well as a science, to acknowledge the seemingly endless difficulties that arise in the application of numerical methods.

Three core competencies are required for the effective use of modeling in crystal growth. One is the thorough grasp of the fundamentals of continuum transport phenomena. The second is the building of an appropriate mathematical model. The third is a general understanding of the numerical methods necessary for solving the governing equations of transport phenomena. For readers interested in more details regarding the comparison of different crystal growth methods, their advantages and disadvantages, we recommend book [9]. A significant advantage of the EFG method, in comparison with the BS method, is that the crystal is grown without interaction with the crucible, which considerably improves the structural quality of the material: there are fewer residual stresses, dislocations, spurious nucleation, or twins. In the case of the BS method, the melt is encapsulated in a crucible,

and the crystallization of the melt takes place in conditions of permanent contact between the melt and the crystal with the inner wall of the crucible (Figure 2). In the case of the EFG method, there is a liquid bridge between the crystal and the shaper (die) called the meniscus. The melt is in a crucible, from which it flows through a capillary tube onto the surface of the shaper (Figures 3–6). Here, a liquid bridge is formed between the shaper surface and the crystal. The crystallization takes place on the so-called "crystallization front", which is the border line between the upper part of the liquid bridge and the bottom of the crystal.

Therefore, the crystal is grown without interaction with the crucible, which considerably improves the structural quality of the material. For more detail, see [10]. "Dewetting" refers to a phenomenon that has occurred spontaneously during many experiments of Bridgman solidification of semiconductors in space (see reviews [11–13]). It also refers to a process developed for crystal growth on Earth (see review in [14]). In both cases, the crystal is grown without interaction with the crucible, which considerably improves the structural quality of the material: there are fewer residual stresses, dislocations, spurious nucleation, or twins. The origin of the gap between the crystal and the crucible comes from a small liquid meniscus at the level of the solid–liquid interface [4]. While this phenomenon is spontaneous under microgravity conditions, because of the lack of hydrostatic pressure, it has been adapted on Earth by applying on the liquid a gas pressure difference, of the order of the hydrostatic pressure, in order to create and maintain the meniscus. For the geometry of the growth system and the main dimensions, angles, temperatures, and pressures of interest in the process, see Figure 7.

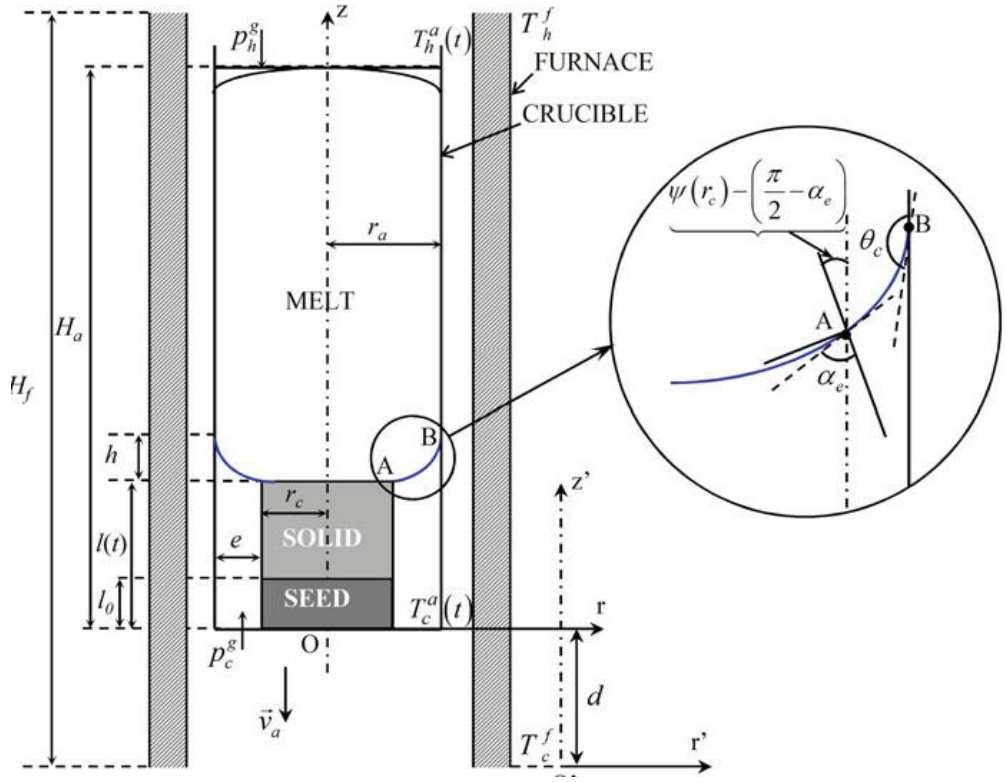


Figure 7. Schematic of the dewetted Bridgman technique.

Many experiments under microgravity have shown that the gap, which is typically smaller than 100 µm, is remarkably constant for several hours of growth. Similarly, dewetted crystals obtained on Earth demonstrate that, under given conditions (essentially a bad wetting of the liquid on the crucible), the crystal radius stays spontaneously constant, while it is almost impossible to obtain a dewetted crystal for other configurations [15,16].

It appears that the process is extremely stable (the grown crystal does not reattach to the crucible wall) in certain cases, while it shows high instability under other conditions. The thin gap thickness is directly linked to the meniscus shape and position, which depend on capillary forces, hydrostatic and hydrodynamic pressures, and heat transfer, all of which likely fluctuate with time. Therefore, in order to master the growth process, it is necessary to perform dynamic stability analysis. Dynamic stability analyses were reported in [17,18].

The micro-pulling-down (μ-PD) technique is a kind of "inverse edge-defined film-fed growth" technique. This means that the melt is pulled downward from a vertical shaper, which is on the bottom part of the crucible. This technique was developed by Fukuda's laboratory in Japan [19–24]. The advantage in the case of the μ-PD technique is that the thermal convection in the liquid bridge (meniscus melt) is zero. The thermal convection can be significant in the case of the edge-defined-film-fed growth technique, even in the case of a static liquid bridge (pulling rate equal to zero). Inequalities presented here are sufficient conditions for the stability or instability of the static liquid bridge appearing in the case of micro-fibers, thin plates, and hollow micro-tube growth using the μ-PD technique. The case in which the contact angle and the growth angle verify the inequality $\alpha_c > \pi/2 - \alpha_g$ is considered. The novelty of this article consists of the obtained inequalities that represent limits for what can and cannot be experimentally achieved with a predetermined material, equipment, and single crystal size. These inequalities can be obtained using second-order conditions for the minimum value of the free energy function. To the best of our knowledge, these types of results have never been published in the literature for materials for which the contact angle and the growth angle verify the inequality $\alpha_c > \pi/2 - \alpha_g$.

In Section 2, the stability or instability of the liquid bridge in the case of micro-fiber growth is analyzed. Section 3 is dedicated to a similar analysis in the case of thin plate growth. Section 4 presents the same kind of analysis in the case of hollow micro-tube growth. In Section 5 we present results, and in Section 6 we offer short comments and conclusions.

We emphasize that this study only investigates the stability and instability of the liquid bridge; our research excludes the study of the growth of shaped single crystals. For this reason, the reference list is short in comparison with the existing literature, and the thermal aspect is completely disregarded.

2. Liquid Bridge in Micro-Fiber Growth

The prototype of an axis-symmetric fiber growth system using the μ-PD technique is represented in Figure 8.

In the hydrostatic approximation, the equation describing the equilibrium capillary surface (shape of the liquid bridge surface) is the Laplace capillary equation (see [25] p. 132). However, to calculate the meniscus shape for the capillary-shaping techniques, it is convenient to employ the Laplace equation in its explicit differential form. To obtain this form of the equation following [25] (p. 132), the variation problem of the total free energy minimum of a liquid column will be solved. For our system, the total free energy is composed of the surface free energy and the gravity field energy. The minimum should be calculated with the additional condition of liquid volume constancy. Solving this problem presents some difficulties. Therefore, our study will be restricted to considering a meniscus (liquid bridge) possessing axial symmetry (see Figure 8 and Formula (1)). Such menisci are obtained during melt pulling of straight circular cylinder-shaped crystals (see [10] p. 24). It should be mentioned that the Laplace capillary equation follows from the necessary condition of the minimum of Function (1). Not all the liquid bridge that represents the solution of the Laplace capillary equation will be stable, i.e., will be physically realized. The stability of this liquid bridge (the static one) should be distinguished from the dynamic stability of the crystallization process. For a statically stable liquid bridge, not only necessary (first order) but also sufficient (second order) conditions of Function (1) should be established. The first-order conditions are the Euler equations, and the second-order conditions are the Jacobi differential equation with the Legendre condition.

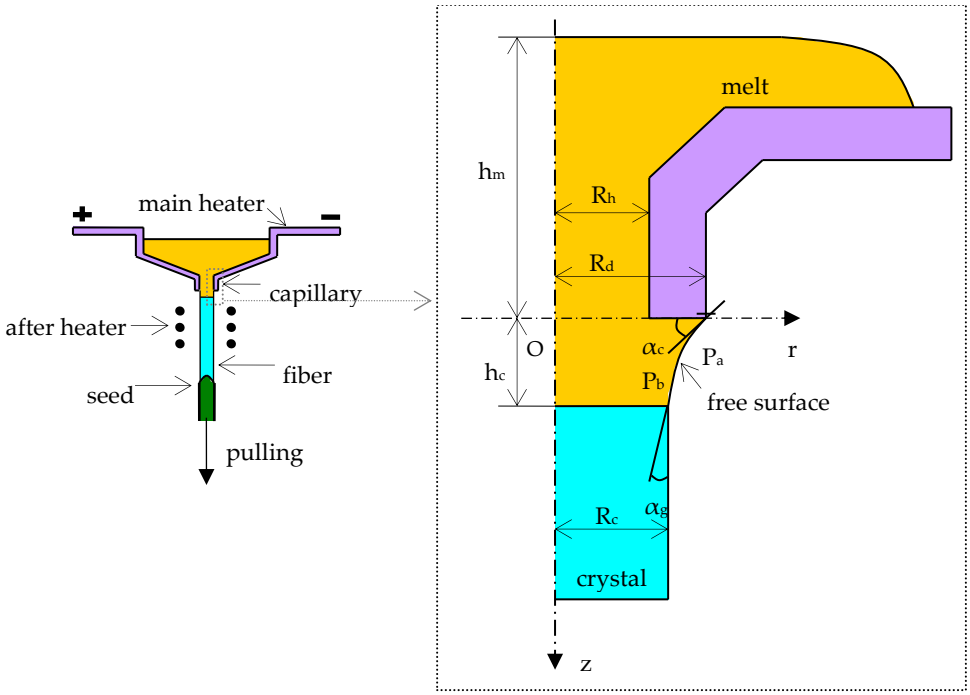


Figure 8. Schematic presentation of an axis-symmetric fiber growth system using the μ-PD technique.

The energy function of the melt column behind the free surface in terms of the meridian curve profile $z(r)$ of the static axis-symmetric liquid bridge is as follows:

$$I(z) = \int_{R_c}^{R_d} \left\{ \gamma \left[1 + (z')^2 \right]^{1/2} - \frac{1}{2} \rho g z^2 - pz \right\} r dr \tag{1}$$

where γ is the melt surface tension, ρ is the melt density, g is the gravity, and $p = -P_a + \rho \cdot g \cdot h_m$ is the pressure difference across the free surface (see [26]).

The stability condition of the axis-symmetric static liquid bridge is that $z(r)$ minimizes (1).

The first-order condition of the minimum value is the Euler equation

$$\frac{d}{dr}\left(\frac{\partial F}{\partial z'}\right) - \frac{\partial F}{\partial z} = 0$$

for the following function:

$$F(z, z', r) = \left\{ \gamma \cdot \left[1 + (z')^2 \right]^{\frac{1}{2}} - \frac{1}{2} \cdot \rho \cdot g \cdot z^2 - p \cdot z \right\} \cdot r$$

In computing the Euler equation for the meridian curve, the following equation is found:

$$z'' = -\frac{\rho g z + p}{\gamma} \left[1 + (z')^2 \right]^{\frac{3}{2}} - \frac{1}{r} \left[1, +, (z')^2 \right] z' \; R_c \le r \le R_d \tag{2}$$

The function $z(r)$ describes the meridian curve profile and verifies the following conditions:

$$z'(R_c) = -\tan\left(\frac{\pi}{2} - \alpha_g\right);\; z(R_c) = h_c > 0 \tag{3}$$

$$z'(R_d) = -\tan \alpha_c;\; z(R_d) = 0 \tag{4}$$

$$z'(r) \text{ is strictly decreasing on } [R_c,\, R_d] \tag{5}$$

The first equality in (3) expresses that at the three-phase point (R_c, h_c), where the thermal condition for solidification is realized (h_c is the meniscus height), the angle between the tangent line to the meridian curve of the free surface and the vertical is equal to the growth angle α_g.

The second equality in (3) expresses that the meniscus meridian curve of the meniscus is fixed to the outer edge of the crystal at the three-phase point (R_c, h_c).

The first equality in (4) expresses that at the outer edge of the shaper, point $(R_d, 0)$, the angle between the tangent line to the meridian curve of the free surface and the horizontal is equal to the contact angle α_c, which is a material "constant" depending on the shaper and the melt.

The second equality in (4) expresses that the meridian curve is fixed at the outer edge of the shaper, i.e., at the point $(R_d, 0)$, where the meridian curve touches the outer edge of the shaper.

Condition (5) concerns the shape of the meridian curve. This formally means $z''(r) < 0$, or concavity. The inequality $\alpha_c > \pi/2 - \alpha_g$ is a consequence of (5).

The analysis of stability of the static liquid bridge in the case $\alpha_c > \pi/2 - \alpha_g$ is justified by the fact that there exist shapes and crystals for which this inequality works and the stability analysis does not exist.

In the case of microfiber growth by the micro-pulling -down method, our understanding of the concavity condition of the meridian curve $z(r)$ is $z''(r) < 0$, i.e., the second derivative is strictly negative. According to this condition, the first-order derivative $z'(r)$ is strictly decreasing. Taking into account Formulas (3) and (4), it follows that $\alpha_c > \pi/2 - \alpha_g$. It can be shown that inequality $\alpha_c > \pi/2 - \alpha_g$ implies the first-order derivative of $z(r)$ is strictly decreasing from where $z''(r) < 0$ in a neighborhood of the point R_d. We point out two things: (a) In Figure 3, a concave meridian curve is represented; in Figures 4–6, convex meridian curves are represented that correspond to the inequality $\alpha_c \leq \pi/2$-α_g. (b) In the case of Figure 1, this kind of understanding of the concepts "concave" and convex is not applicable; that is, because the curve represented in Figure 1 is not the graphic of the function $z(r)$. In the case of Figure 1, to a value of r corresponds two values for z; one is situated in the upper half part of the curve, which is concave, and the other value is situated in the lower half part of the curve, which is convex.

In case of convex liquid bridges, $\alpha_c \leq \pi/2 - \alpha_g$ the second-order derivative of the function $z(r)$ is strictly positive, and the first-order derivative of $z(r)$ is strictly increasing. The stability of the static liquid bridge in the $\alpha_c \leq \pi/2 - \alpha_g$ case was analyzed in [26,27]. The stability of the liquid bridge in the $\alpha_c > \pi/2 - \alpha_g$ case is an open problem.

Using (2)–(5) and the concavity condition for $z(r)$ ($z''(r) < 0$), the following inequalities can be determined:

$$\begin{gathered}\gamma \cdot \frac{\alpha_c + \alpha_g - \frac{\pi}{2}}{R_d} \cdot \frac{n}{n-1} \cdot \cos\alpha_c - \frac{\rho \cdot g}{R_d} \cdot \frac{(n-1)}{n} \cdot \tan\alpha_c + \frac{\gamma}{R_d} \cdot \cos\alpha_g \leq \\ p \leq \gamma \cdot \frac{\alpha_c + \alpha_g - \frac{\pi}{2}}{R_d} \cdot \frac{n}{n-1} \cdot \sin\alpha_g + \frac{\gamma}{R_d} \cdot n \cdot \sin\alpha_c\end{gathered} \tag{6}$$

where $n = \frac{R_d}{R_c} > 1$.

Inequalities (6) are necessary conditions for the existence of $z(r)$. This has to be verified by pressure difference $p = -P_a + \rho \cdot g \cdot h_m$. For stability or instability of the liquid bridge, the second-order conditions of the minimum of (1), i.e., the Legendre condition $\frac{\partial^2 F}{\partial z' \partial z'} \geq 0$ and the Jacobi equation

$$\frac{d}{dr}\left[\frac{\partial^2 F}{\partial z' \partial z'} \cdot z'\right] - \left[\frac{\partial^2 F}{\partial z \partial z} - \frac{d}{dr}\left(\frac{\partial^2 F}{\partial z' \partial z}\right)\right] \cdot \eta = 0$$

have to be analyzed.

The Legendre condition in this case is the inequality:

$$r \cdot \gamma \left[1 + (z')^2\right]^{-\frac{3}{2}} \geq 0 \tag{7}$$

which is obviously verified. The Jacobi equation in this case is the following:

$$(r \cdot \gamma[1 + (z')^2]^{-\frac{3}{2}} \cdot z')' + \rho \cdot g \cdot r \cdot \eta = 0 \tag{8}$$

To obtain a stability result for the liquid bridge, it is sufficient to identify a "Sturm-type upper bound" ([27] Chapter 11) for the Jacobi Equation (8). For this purpose, we note that the following inequalities concerning the coefficients of Equation (8) hold:

$$r \cdot \gamma[1 + (z')^2]^{-\frac{3}{2}} \geq \frac{R_d \cdot \gamma}{n} \cdot \cos^3 \alpha_c, \rho \cdot g \cdot r \leq \rho \cdot g \cdot R_d \tag{9}$$

It follows that the equation as follows:

$$[\frac{R_d \cdot \gamma}{n} \cdot \cos^3 \alpha_c] \cdot \xi'' + [\rho \cdot g \cdot R_d] \cdot \xi = 0 \tag{10}$$

Is a "Sturm-type upper bound" for Equation (8). An arbitrary solution of Equation (10) is of the form $\xi(r) = A \cdot \sin(\omega t + \phi)$, where A and ϕ are arbitrary constants and $\omega^2 = \frac{\rho \cdot g \cdot n}{\gamma \cdot \cos^3 \alpha_c}$. The half period of any non-zero solution of (10) is $\frac{\pi}{\omega} = \pi \cdot \frac{\gamma^{1/2} \cdot \cos^{3/2} \alpha_c}{\rho^{1/2} \cdot n^{1/2} \cdot g^{1/2}}$. If the half period is more than $R_d - R_c$, then any non-zero solution of (10) vanishes at most once on the interval $[R_c, R_d]$.

In other words, if the following inequality holds $\frac{n-1}{n^{1/2}} < \pi \cdot \frac{1}{R_d} \cdot \frac{\gamma^{1/2} \cdot \cos^{3/2} \alpha_c}{\rho^{1/2} \cdot g^{1/2}}$, then any non-zero solution $\xi(r)$ of (10) vanishes at most once on the interval $[R_c, R_d]$. Hence, according to [27] Chapter 11, the solution $\eta(r)$ of the Jacobi equation that verifies $\eta(R_d) = 0$ and $\eta'(R_d) = 1$ has only one zero on the interval $[R_c, R_d]$. This means that the Jacobi condition for the weak minimum value is verified (see [27]).

Theorem 1. *If for* $n = \frac{R_d}{R_c} > 1$ *the following inequality holds:*

$$\frac{n-1}{n^{1/2}} < \pi \cdot \frac{1}{R_d} \cdot \frac{\gamma^{1/2} \cdot \cos^{3/2} \alpha_c}{\rho^{1/2} \cdot g^{1/2}} \tag{11}$$

then the liquid bridge is stable.

To obtain instability results for the Jacobi equation, a "Sturm-type lower bound equation" ([27] Chapter 11) has to be found. For this purpose, we note that for the coefficients of the Jacobi equation, the following inequalities hold:

$$r \cdot \gamma[1 + (z')^2]^{-\frac{3}{2}} \leq R_d \gamma \cdot \sin^3 \alpha_g, \ \rho \cdot g \cdot r \geq \rho \cdot g \cdot R_d / n \tag{12}$$

It follows that the following equation:

$$[R_d \cdot \gamma \cdot \sin^3 \alpha_g] \cdot \varsigma'' + [\rho \cdot g \cdot R_d / n] \cdot \zeta = 0 \tag{13}$$

is a "Sturm-type lower bound equation" for the Jacobi Equation (8). An arbitrary solution of Equation (13) is of the form $\zeta(r) = A \cdot \sin(\omega t + \phi)$, where A and ϕ are arbitrary constants and $\omega^2 = \frac{\rho \cdot g}{n \cdot \gamma \cdot \sin^3 \alpha_g}$. The period of any non-zero solution of (13) is $\frac{2 \cdot \pi}{\omega} = 2 \cdot \pi \cdot \frac{\gamma^{1/2} \cdot n^{1/2} \cdot \sin^{3/2} \alpha_g}{\rho^{1/2} \cdot g^{1/2}}$. If the period is less than $R_d - R_c$, then any non-zero solution of (13) vanishes at least twice on the interval $[R_c, R_d]$. In other words, if the inequality $\frac{n-1}{n^{3/2}} > 2 \cdot \pi \cdot \frac{1}{R_d} \cdot \frac{\gamma^{1/2} \cdot \sin^{3/2} \alpha_g}{\rho^{1/2} \cdot g^{1/2}}$ holds, then any non-zero solution $\zeta(r)$ of (13) vanishes at least twice on the interval $[R_c, R_d]$.

Hence, according to [27] Chapter 11, the solution $\eta(r)$ of the Jacobi equation that verifies $\eta(R_d) = 0$ and $\eta'(R_d) = 1$ vanishes at least twice on the interval $[R_c, R_d]$. This means that the Jacobi condition for the weak minimum value is not satisfied (see [27]).

Theorem 2. *If for* $n = \frac{R_d}{R_c} > 1$ *the following inequality holds:*

$$\frac{n-1}{n^{3/2}} > 2 \cdot \pi \cdot \frac{1}{R_d} \cdot \frac{\gamma^{1/2} \cdot \sin^{3/2} \alpha_g}{\rho^{1/2} \cdot g^{1/2}} \tag{14}$$

then the liquid bridge is unstable.

3. Liquid Bridge in Thin Plate Growth

The prototype of a YOZ plane-symmetric plate growth system using the μ-PD technique is represented in Figure 9.

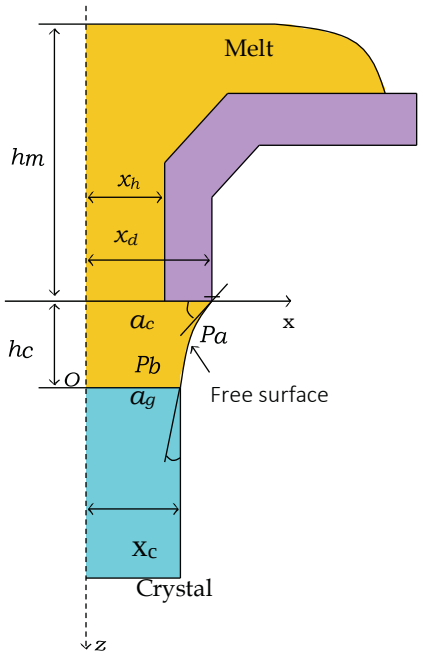


Figure 9. Schematic presentation of a YOZ-plane symmetric plate growth system using the μ-PD method.

In this case, the energy function of the melt column behind the liquid bridge-free surface in terms of the liquid bridge profile curve $z(x)$ is the following:

$$I(z) = \int_{x_c}^{x_d} \left\{ \gamma \cdot \left[1 + (z')^2\right] \frac{1}{2} - \frac{1}{2} \cdot \rho \cdot g \cdot z^2 - p \cdot z \right\} dx \tag{15}$$

with $p = -P_a + \rho \cdot g \cdot h_m$ (see [28]).

The stability condition of the YOZ plane-symmetric static liquid bridge is that $z(x)$ minimizes (15). The first-order condition of the minimum is the Euler equation

$$\frac{d}{dx}\left(\frac{\partial F}{\partial z'}\right) - \frac{\partial F}{\partial z} = 0$$

for the following function:

$$F(z, z', x) = \left\{ \gamma \cdot \left[1 + (z')^2\right]^{\frac{1}{2}} - \frac{1}{2} \cdot \rho \cdot g \cdot z^2 - p \cdot z \right\}$$

Computing the Euler equation in this case for the liquid bridge profile curve, the following Equation is found:

$$z'' = -\frac{\rho \cdot g \cdot z + p}{\gamma}\left[1 + \left(z'\right)^2\right]^{3/2}; x_c \leq x \leq x_d \tag{16}$$

The function $z(x)$ describing the profile curve has to verify the following boundary conditions:

$$z'(x_c) = -\tan\left(\pi/2 - \alpha_g\right);\ z(x_c) = h_c > 0 \tag{17}$$

$$z'(x_d) = -\tan\alpha_c;\ z(x_d) = 0 \tag{18}$$

$$z'(r) \text{ is strictly decreasing on } [x_c,\ x_d] \tag{19}$$

Using (16)–(19) and the concavity condition for $z(x)$ ($z''(x) < 0$), the following inequalities can be found:

$$\begin{gathered}\gamma \cdot \frac{\alpha_c + \alpha_g - \frac{\pi}{2}}{x_d} \cdot \frac{n}{n-1} \cdot \cos\alpha_c - \frac{\rho \cdot g}{x_d} \cdot \frac{(n-1)}{n} \cdot \tan\alpha_c \leq \\ p \leq \gamma \cdot \frac{\alpha_c + \alpha_g - \frac{\pi}{2}}{x_d} \cdot \frac{n}{n-1} \cdot \sin\alpha_g\end{gathered} \tag{20}$$

where $n = \frac{x_d}{x_c} > 1$. Inequalities (20) represent necessary conditions for the existence of $z(x)$. The pressure difference $p = -P_a + \rho \cdot g \cdot h_m$ has to verify (20). For stability or instability of the liquid bridge, the second-order conditions of the minimum of (16), i.e., the Legendre condition

$$\frac{\partial^2 F}{\partial z' \partial z'} \geq 0$$

and the Jacobi equation

$$\frac{d}{dx}\left[\frac{\partial^2 F}{\partial z' \partial z'} \cdot \eta'\right] - \left[\frac{\partial^2 F}{\partial z \partial z} - \frac{d}{dx}\left(\frac{\partial^2 F}{\partial z \partial z'}\right)\right] \cdot \eta = 0$$

have to be analyzed.

The Legendre condition in this case is the following inequality:

$$\gamma\left[1 + \left(z'\right)^2\right]^{-\frac{3}{2}} \geq 0 \tag{21}$$

which is obviously verified.

The Jacobi equation in this case is the following equation:

$$\left(\gamma\left[1 + \left(z'\right)^2\right]^{-\frac{3}{2}} \cdot \eta'\right)' + \rho \cdot g \cdot \eta = 0 \tag{22}$$

We note that the following inequalities concerning the coefficients of Equation (22) hold:

$$\gamma\left[1 + \left(z'\right)^2\right]^{-\frac{3}{2}} \geq \gamma \cdot \cos^3\alpha_c;\ \rho \cdot g \leq \rho \cdot g \tag{23}$$

Therefore, the following equation:

$$\left[\gamma \cdot \cos^3\alpha_c\right] \cdot \xi'' + \left[\rho \cdot g\right] \cdot \xi = 0 \tag{24}$$

is a "Sturm-type upper bound" for Equation (22). Hence, the conclusion follows:

Theorem 3. *If for* $n = \frac{x_d}{x_c} > 1$ *the following inequality holds:*

$$\frac{n-1}{n} < \pi \cdot \frac{1}{x_d} \cdot \frac{\gamma^{1/2} \cdot \cos^{3/2}\alpha_c}{\rho^{1/2} \cdot g^{1/2}} \tag{25}$$

then the liquid bridge is stable.

Analogously, the following equation:

$$[\gamma \cdot \sin^3 \alpha_g] \cdot \zeta'' + [\rho \cdot g] \cdot \zeta = 0 \tag{26}$$

is a "Sturm-type lower bound" for Equation (23). Hence, the conclusion follows:

Theorem 4. *If for* $n = \frac{x_d}{x_c} > 1$ *the following, inequality holds*:

$$\frac{n-1}{n} > 2 \cdot \pi \cdot \frac{1}{x_d} \cdot \frac{\gamma^{1/2} \cdot \sin^{3/2} \alpha_g}{\rho^{1/2} \cdot g^{1/2}} \tag{27}$$

then the liquid bridge is unstable.

4. Liquid Bridge in Thin Hollow Tube Growth

The prototype of an axis-symmetric hollow tube growth system using the μ-PD technique is represented in Figure 10.

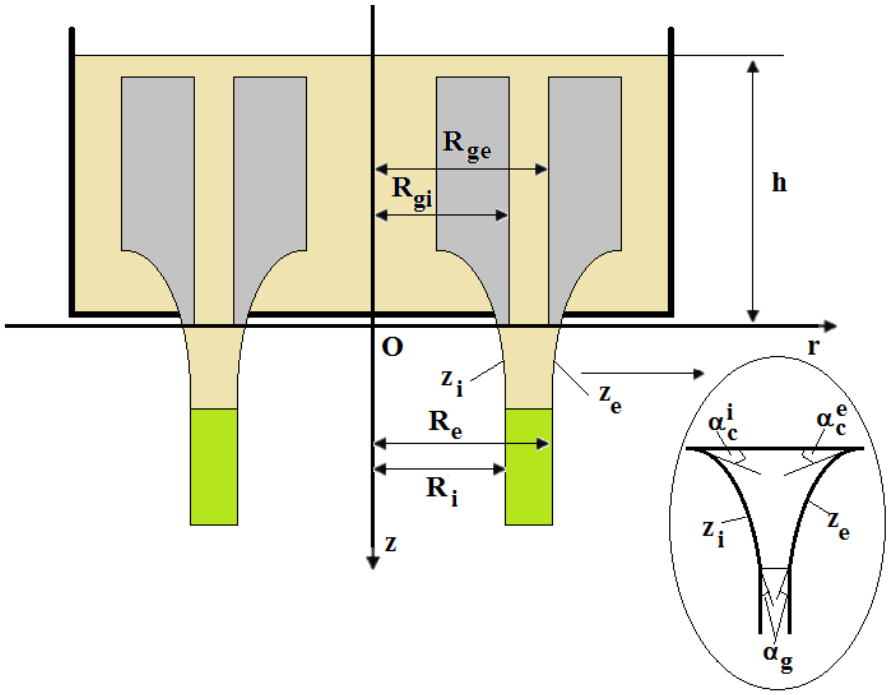


Figure 10. Schematic presentation of an axis-symmetric hollow tube growth system using the μ-PD method.

In the case of the hollow tube growth method, there exist two independent liquid bridges: one in the interior of the tube and one on the exterior of the tube. The meridian curve of the bridge located in the interior of the tube is denoted by $z_i(r)$, and the meridian curve of the bridge located on the exterior of the tube is denoted by $z_e(r)$. In terms of these meridian curves, the functional energies of the melt columns behind the liquid bridge-free surface area are as follows (see [29]):

$$I_i(z_i) = \int_{R_{gi}}^{R_{ci}} \left\{ \gamma \cdot \left[1 + (z_i')^2 \right]^{\frac{1}{2}} - \frac{1}{2} \cdot \rho \cdot g \cdot z_i^2 - p_i \cdot z_i \right\} \cdot r \cdot dr \tag{28}$$

$$I_e(z_e) = \int_{Rce}^{R_{ge}} \left\{ \gamma \cdot \left[1 + \left(z_e'\right)^2\right]^{\frac{1}{2}} - \frac{1}{2} \cdot \rho \cdot g \cdot z_e^2 - p_e \cdot z_e \right\} \cdot r \cdot dr \tag{29}$$

The stability condition of the axis-symmetric static liquid bridges is that $z_i(x)$ minimizes (28) and $z_e(x)$ minimizes (29).

The first-order necessary condition of the minimum is the Euler equation

$$\frac{d}{dx}\left(\frac{\partial F}{\partial z'}\right) - \frac{\partial F}{\partial z} = 0$$

for the following functions:

$$F_i(z_i, z_i', r) = \left\{ \gamma \cdot \left[1 + \left(z_i'\right)^2\right]^{\frac{1}{2}} - \frac{1}{2} \cdot \rho \cdot g \cdot z_i^2 - p_i \cdot z_i \right\} \cdot r$$

$$F_e(z_e, z_e', r) = \left\{ \gamma \cdot \left[1 + \left(z_e'\right)^2\right]^{\frac{1}{2}} - \frac{1}{2} \cdot \rho \cdot g \cdot z_e^2 - p_e \cdot z_e \right\} \cdot r$$

with $p_i = -P_i^a + \rho \cdot g \cdot h$ and $p_e = -P_e^a + \rho \cdot g \cdot h$.

Computing the Euler equation in this case for the interior and exterior liquid bridge profile curves, the following equations are found:

$$z_i'' = -\frac{\rho \cdot g \cdot z_i + p_i}{\gamma}\left[1 + \left(z_i'\right)^2\right]^{\frac{3}{2}} - \frac{1}{r} \cdot \left[1 + \left(z_i'\right)^2\right] \cdot z_i'; R_{gi} \le r \le R_{ci} \tag{30}$$

$$z_e'' = -\frac{\rho \cdot g \cdot z_e + p_e}{\gamma}\left[1 + \left(z_e'\right)^2\right]^{\frac{3}{2}} - \frac{1}{r} \cdot \left[1 + \left(z_e'\right)^2\right] \cdot z_e';\ R_{ce} \le r \le R_{ge} \tag{31}$$

Here, R_{gi}, R_{ge} represent the inner and outer radii of the shaper, respectively; R_{ci}, R_{ce} represent the inner and outer radii of the tube being grown, respectively, and satisfy the following:

$$0 < R_{gi} < R_{ci} < (R_{gi} + R_{ge})/2 < R_{ce} < R_{ge}$$

The function $z_i(r)$ describes the interior bridge meridian curve profile and verifies the following boundary conditions:

$$z_i'(R_{ci}) = \tan\left(\pi/2 - \alpha_g\right);\ z_i(R_{ci}) = h_i^c > 0. \tag{32}$$

$$z_i'\left(R_{gi}\right) = \tan\,\alpha_c;\ z_i\left(R_{gi}\right) = 0. \tag{33}$$

$$z' \text{ is strictly increasing on } \left[R_{gi},\ R_{ci}\right] \tag{34}$$

The function $z_e(r)$ describes the exterior bridge meridian curve profile and verifies the following boundary conditions:

$$z_e'(R_{ce}) = -\tan\left(\pi, /, 2, -, \alpha_g\right);\ z_e(R_{ce}) = h_e^c > 0. \tag{35}$$

$$z_e'\left(R_{ge}\right) = -\tan\,\alpha_c;\ z_e\left(R_{ge}\right) = 0 \tag{36}$$

$$z' \text{ is strictly decreasing on } \left[R_{ce},\ R_{ge}\right]. \tag{37}$$

Using (30), (32)–(34), and the concavity condition for $z_i(r)$ ($z_i''(r) < 0$), the following inequalities can be found:

$$\gamma \cdot \frac{\alpha_c+\alpha_g-\pi/2}{R_{gi}} \cdot \frac{1}{m-1} \cdot \cos\,\alpha_c - \rho \cdot g \cdot R_{gi} \cdot (m-1) \cdot \tan\alpha_c - \frac{\gamma}{R_{gi}} \cdot \sin\alpha_c \le p_i \le \gamma \cdot \frac{\alpha_c+\alpha_g-\pi/2}{R_{gi}} \cdot \frac{1}{m-1} \cdot \sin\,\alpha_g - \frac{\gamma}{R_{gi}} \cdot \frac{1}{m} \cdot \cos\alpha_g \tag{38}$$

where $R_{ci}/R_{gi} = m > 1$.

Using (30), (35)–(37), and the concavity condition for $z_e(r)$ ($z_e''(r) < 0$), the following inequalities can be found:

$$\gamma \cdot \frac{\alpha_c+\alpha_g-\frac{\pi}{2}}{R_{ge}} \cdot \frac{n}{n-1} \cdot \cos\,\alpha_c - \frac{\rho \cdot g}{R_{ge}} \cdot \frac{(n-1)}{n} \cdot \tan\,\alpha_c + \frac{\gamma}{R_{ge}} \cdot \cos\,\alpha_g \le p_e \le \gamma \cdot \frac{\alpha_c+\alpha_g-\frac{\pi}{2}}{R_{ge}} \cdot \frac{n}{n-1} \cdot \sin\,\alpha_g + \frac{\gamma}{R_{ge}} \cdot n \cdot \sin\,\alpha_c \tag{39}$$

where $n = R_{ge}/R_{ce} > 1$.

Inequalities (38) and (39) represent necessary conditions for the existence of $z_i(r)$ and $z_e(r)$. The pressure differences $p_i = -P_i^a + \rho \cdot g \cdot h$ and $p_e = -P_e^a + \rho \cdot g \cdot h$ have to verify these inequalities. For stability or instability of the interior and exterior liquid bridge, the second-order conditions of the minima of (28) and (29), i.e., the Legendre condition

$$\frac{\partial^2 F}{\partial z' \partial z'} \ge 0$$

and the Jacobi equation

$$\frac{d}{dr}\left[\frac{\partial^2 F}{\partial z' \partial z'} \cdot \eta'\right] - \left[\frac{\partial^2 F}{\partial z \partial z} - \frac{d}{dr}\left(\frac{\partial^2 F}{\partial z \partial z'}\right)\right] \cdot \eta = 0$$

have to be analyzed for the following functions:

$$F_i(z_i, z_i{}', r) = \left\{ \gamma \cdot \left[1 + \left(z_i{}'\right)^2\right]^{\frac{1}{2}} - \frac{1}{2} \cdot \rho \cdot g \cdot z_i^2 - p_i \cdot z_i \right\} \cdot r$$

$$F_e(z_e, z_e{}', r) = \left\{ \gamma \cdot \left[1 + \left(z_e{}'\right)^2\right]^{\frac{1}{2}} - \frac{1}{2} \cdot \rho \cdot g \cdot z_e^2 - p_e \cdot z_e \right\} \cdot r$$

The Legendre conditions for the interior and exterior bridges are the following:

$$\frac{\partial^2 F_i}{\partial z_i' \, \partial z_i'} = \gamma \cdot [1 + (z_i{}')^2]^{-3/2} \cdot r \ge 0, r \in \left[R_{gi},\ R_{ci}\right]$$

$$\frac{\partial^2 F_e}{\partial z_e' \partial z_e'} = \gamma \cdot [1 + (z_{ei}{}')^2]^{-3/2} \cdot r \ge 0, r \in \left[R_{ce},\ R_{ge}\right]$$

We note that these conditions are obviously verified.

The Jacobi equations for the interior and exterior liquid bridges are as follows:

$$\gamma \cdot \frac{d}{dr}[1 + (z_i{}')^2]^{-3/2} \cdot r \cdot \xi'] + \rho \cdot g \cdot r \cdot \xi = 0 \; r \in \left[R_{gi},\ R_{ci}\right] \tag{40}$$

$$\gamma \cdot \frac{d}{dr}\left[1 + \left(z_e{}'\right)^2\right]^{-3/2} \cdot r \cdot \zeta'] + \rho \cdot g \cdot r \cdot \zeta = 0 \; r \in \left[R_{ce},\ R_{ge}\right] \tag{41}$$

For the Jacobi equation in the case of the interior liquid bridge (40), the following Equation (42):

$$\gamma \cdot \frac{d}{dr}[R_{gi} \cdot \cos^3\alpha_c \cdot \xi'] + \rho \cdot g \cdot R_{ci} \cdot \xi = 0 \tag{42}$$

is a Sturm-type upper bound, and the Equation (43)

$$\gamma \cdot \frac{d}{dr}[R_{ci} \cdot \sin^3 \alpha_g \cdot \zeta'] + \rho \cdot g \cdot R_{gi} \cdot \zeta = 0 \tag{43}$$

is a Sturm-type lower bound. Therefore, for the inner liquid bridge, the following conclusion holds:

Theorem 5. *If for $m = R_{ci}/R_{gi}$ the following, inequality holds:*

$$(m-1) \cdot m^{1/2} < \frac{\pi}{R_{gi}} \cdot \frac{\gamma^{1/2} \cos \alpha_c^{3/2}}{\rho^{1/2} \cdot g^{1/2}} \tag{44}$$

then the internal liquid bridge is stable.

If for $m = R_{ci}/R_{gi}$ the following inequality holds:

$$(m-1) \cdot m^{-1/2} > \frac{2\pi}{R_{gi}} \cdot \frac{\gamma^{1/2} \sin^{3/2} \alpha_g}{\rho^{1/2} \cdot g^{1/2}} \tag{45}$$

then the internal liquid bridge is unstable.

In the case of the exterior liquid bridge for the Jacobi Equation (41), the following Equation (46):

$$\gamma \cdot \frac{d}{dr}[R_{ce} \cdot \cos^3 \alpha_c \cdot \xi'] + \rho \cdot g \cdot R_{ge} \cdot \xi = 0 \tag{46}$$

is a Sturm-type upper bound, and the following Equation (47):

$$\gamma \cdot \frac{d}{dr}[R_{ge} \cdot \sin^3 \alpha_g \cdot \zeta'] + \rho \cdot g \cdot R_{ce} \cdot \zeta = 0 \tag{47}$$

is a Sturm-type lower bound. Therefore, for the exterior liquid bridge, the following conclusion holds:

Theorem 6. *If for $n = R_{ge}/R_{ce}$ the following, inequality holds:*

$$(n-1) \cdot n^{-1/2} < \frac{\pi}{R_{ge}} \cdot \frac{\gamma^{1/2} \cos \alpha_c^{3/2}}{\rho^{1/2} \cdot g^{1/2}} \tag{48}$$

then the external liquid bridge is stable.

If for $n = R_{ge}/R_{ce}$ the following inequality holds:

$$(n-1) \cdot n^{-3/2} > \frac{2\pi}{R_{ge}} \cdot \frac{\gamma^{1/2} \sin \alpha_g^{3/2}}{\rho^{1/2} \cdot g^{1/2}} \tag{49}$$

then the external liquid bridge is unstable.

5. Results

In the case of thin fibers for liquid bridges, the following results hold:

- If, for $n = \frac{R_d}{R_c} > 1$ the inequality $\frac{n-1}{n^{1/2}} < \pi \cdot \frac{1}{R_d} \cdot \frac{\gamma^{1/2} \cdot \cos^{3/2} \alpha_c}{\rho^{1/2} \cdot g^{1/2}}$ holds, then the liquid bridge is stable.
- If, for $n = \frac{R_d}{R_c} > 1$ the inequality $\frac{n-1}{n^{3/2}} > 2 \cdot \pi \cdot \frac{1}{R_d} \cdot \frac{\gamma^{1/2} \cdot \sin^{3/2} \alpha_g}{\rho^{1/2} \cdot g^{1/2}}$ holds, then the liquid bridge is unstable.

In the case of thin plates for liquid bridges, the following results hold:

- If for $n = \frac{x_d}{x_c} > 1$ the inequality $\frac{n-1}{n} < \pi \cdot \frac{1}{x_d} \cdot \frac{\gamma^{1/2} \cdot \cos^{3/2} \alpha_c}{\rho^{1/2} \cdot g^{1/2}}$ holds, then the liquid bridge is stable.
- If for $n = \frac{x_d}{x_c} > 1$ the inequality $\frac{n-1}{n} > 2 \cdot \pi \cdot \frac{1}{x_d} \cdot \frac{\gamma^{1/2} \cdot \sin^{3/2} \alpha_g}{\rho^{1/2} \cdot g^{1/2}}$ holds, then the liquid bridge is unstable.

In the case of thin hollow tubes for liquid bridges, the following results hold:

- If for $m = R_{ci}/R_{gi}$ the inequality $(m-1) \cdot m^{1/2} < \frac{\pi}{R_{gi}} \cdot \frac{\gamma^{1/2} \cos \alpha_c^{3/2}}{\rho^{1/2} \cdot g^{1/2}}$ holds, then the internal liquid bridge is stable.
- If for $m = R_{ci}/R_{gi}$ the inequality $(m-1) \cdot m^{-1/2} > \frac{2\pi}{R_{gi}} \cdot \frac{\gamma^{1/2} \sin^{3/2} \alpha_g}{\rho^{1/2} \cdot g^{1/2}}$ holds, then the internal liquid bridge is unstable.
- If for $n = R_{ge}/R_{ce}$ the inequality $(n-1) \cdot n^{-1/2} < \frac{\pi}{R_{ge}} \cdot \frac{\gamma^{1/2} \cos \alpha_c^{3/2}}{\rho^{1/2} \cdot g^{1/2}}$ holds, then the external liquid bridge is stable.
- If for $n = R_{ge}/R_{ce}$ the inequality $(n-1) \cdot n^{-3/2} > \frac{2\pi}{R_{ge}} \cdot \frac{\gamma^{1/2} \sin \alpha_g^{3/2}}{\rho^{1/2} \cdot g^{1/2}}$ holds, then the external liquid bridge is unstable.

6. Comments and Conclusions

(i) In the case of materials for which $\alpha_c \leq \pi/2 - \alpha_g$ in papers [26,28–31], sufficient conditions for the theoretical existence and static stability of liquid bridges in thin fiber, thin plate, and thin hollow tube growth by the PD method were reported. If the sufficient conditions for stability of liquid bridges reported in [26,28,29] are not verified, this does not imply that the liquid bridge is unstable. As far as we know, there are no instability results reported in the literature for the $\alpha_c \leq \pi/2 - \alpha_g$ case.

In the case of materials for which $\alpha_c \leq \pi/2 - \alpha_g$ in [32–34], the dynamics of the growth process of thin fiber, thin plate, and thin hollow tube are described when the liquid bridge is stable. In these papers, the flow field, the thermal field, and the impurity distributions are also computed and numerical simulations are provided.

(ii) In the case of materials for which $\alpha_c > \pi/2 - \alpha_g$, our findings reveal sufficient conditions for the stability or instability of a static liquid bridge appearing in the case of thin fiber, thin plate, and thin hollow tube growth by the pulling-down method. The imposed boundary conditions originate in crystal growth. If the reported sufficient condition of stability of the liquid bridge is not verified, this does not imply that the liquid bridge is unstable. The main novelty in this article consists in the obtained inequalities. These represent limits for what can and cannot be achieved. Experimentally, only stable static liquid bridges can be created. Unstable static liquid bridges exist just in theory; in reality, they collapse; therefore, they are not appropriate for crystal growth.

Author Contributions: Conceptualization, A.V.C. and S.B.; Formal analysis, S.B.; Writing—original draft, A.V.C. All authors have read and agreed to the published version of the manuscript.

Funding: This research did not receive any specific grant from funding agencies in the public, commercial, or not-for-profit sectors.

Data Availability Statement: The original contributions presented in the study are included in the article, further inquiries can be directed to the corresponding author.

Conflicts of Interest: The authors declare no conflicts of interest.

References

1. Kostoglou, M.; Karapantsios, T.D. On the identification of liquid surface properties using liquid bridges. *Adv. Colloid Interface Sci.* **2015**, *222*, 436–445. [CrossRef] [PubMed]
2. Roisman, V.; Abboud, M.; Brockmann, P.; Berner, F.; Berger, R.; Brumm, P.R.; Sauer, H.M.; Dörsam, E.; Hussong, J. Forced flows in liquid bridges. *Curr. Opin. Colloid Interface Sci.* **2023**, *67*, 101738. [CrossRef]

3. Gómez, F.G.; Flórez, V.M.; Morales, M.; Blanco, A.; López, C. Colloidal crystals and water: Perspectives on liquid–solid nanoscale phenomena in wet particulate media. *Adv. Colloid Interface Sci.* **2016**, *234*, 142–160. [CrossRef] [PubMed]
4. Morawetz, K. Theory of water and charged liquid bridges. *Phys. Rev. A At. Mol. Opt. Phys.* **2012**, *86*, 026302. [CrossRef] [PubMed]
5. Peregrine, D.H.; Shoker, G.; Symon, A. *The Bifurcation of Liquid Bridges*; Cambridge University Press: Cambridge, UK, 2006.
6. Huang, C.H.; Carvalho, M.S.; Kumar, S. Stretching liquid bridges with moving contact lines: Comparison of liquid-transfer predictions and experiments. *Soft Matter* **2016**, *12*, 7457–7469. [CrossRef] [PubMed]
7. Mastrangeli, M. *The Fluid Joint: The Soft Spot of Micro- and Nanosystems*; WILEY-VCH: Hoboken, NJ, USA, 2015. [CrossRef]
8. Meseguer, J.; Slobozhanin, L.A.; Perales, J.M. A Review on the Stability of Liquid Bridges. *Adv. Space Res.* **1995**, *16*, 5–14. [CrossRef]
9. Dhanaraj, G.; Byrappa, K.; Prasad, V.; Dudley, M. (Eds.) *Springer Handbook of Crystal Growth*; Springer: Berlin/Heidelberg, Germany, 2010.
10. Tatarchenko, V.A. *Shaped Crystal Growth*; Kluwer Academic Publishers: Philip Drive Norwell, MA, USA, 1993.
11. Wilcox, W.R.; Regel, L.L. Detached solidification in microgravity—A review. *Microgravity Sci. Technol.* **1998**, *11*, 152–166.
12. Duffar, T. Bulk crystal growth under microgravity conditions. In *Bulk Crystal Growth of Electronic, Optical and Optoelectronics Materials*; Capper, P., Ed.; Wiley: Chichester, UK, 2005; pp. 477–524.
13. Duffar, T.; Boiton, P.; Dusserre, P.; Abadie, J. Crucible de-wetting during Bridgman growth in microgravity. II. Smooth crucibles. *J. Cryst. Growth* **1997**, *179*, 397–409. [CrossRef]
14. Duffar, T.; Sylla, L. Vertical Bridgman and dewetting. In *Crystal Growth Processes Based on Capillarity*; Duffar, T., Ed.; Wiley-Blackwell: Hoboken, NJ, USA, 2010; pp. 355–408. ISBN 978-0-470-71244-3.
15. Sylla, L.; Paulin, J.P.; Vian, G.; Garnier, C.; Duffar, T. Effect of residual impurities on the dewetting of antimonide melts in fused silica crucibles in the case of bulk crystal growth. *Mater. Sci. Eng. A* **2008**, *495*, 208–214. [CrossRef]
16. Sylla, L. Etude Expérimentale et Thermodynamique du Pocédé de Démouillage Appliqué aux Semiconducteurs. Ph.D. Thesis, Grenoble Institute of Technology, Saint-Martin-d'Hères, France, 2008. (In French).
17. Balint, S.; Epure, S.; Duffar, T.; Braescu, L. Dewetted Bridgman crystal growth: Practical stability over a bounded time period in a forced regime. *J. Eng. Math.* **2012**, *75*, 191–208. [CrossRef]
18. Balint, S.; Epure, S. Non-Lyapunov Type Stability in a Model of the Dewetted Bridgman Crystal Growth under Zero Gravity Conditions. *Microgravity Sci. Technol.* **2011**, *23* (Suppl. S1), S49–S58. [CrossRef]
19. Fukuda, T.; Chani, V.I. (Eds.) Shaped Crystals: Growth by Micro-Pulling-down Technique. Springer: New York, NY, USA, 2007.
20. Yoshikawa, A.; Chani, V.I. Growth of Optical Crystals by the Micro-Pulling-down Method. *MRS Bull.* **2009**, *34*, 266–270. [CrossRef]
21. Fukuda, T.; Rudolf, R.; Uda, S. (Eds.) *Fiber Crystal Growth from the Melt*; Springer: New York, NY, USA, 2004. [CrossRef]
22. Zhuravleva, M.; Chani, V.I.; Yanagida, T.; Yoshikawa, A. The micro-pulling-down growth of $Bi_4Si_3O_{12}$ (BSO) and $Bi_4Ge_3O_{12}$ (BGO) fiber crystals and their scintillation efficiency. *J. Crystal Growth* **2008**, *310*, 2152–2156. [CrossRef]
23. Yokota, Y.; Chani, V.I.; Sato, M.; Tota, K.; Onodera, K.; Yanagida, T.; Yoshikawa, A. Growth and crystallinity of shaped and multiple sapphire crystals by a micro-pulling-down method. *J. Crystal Growth* **2011**, *318*, 983–986. [CrossRef]
24. Yokota, Y.; Tanaka, H.; Sato, M.; Chani, V.; Tota, K.; Onodera, K.; Yanagida, T.; Yoshikawa, A. Growth and Characterization of Shape-Controlled Single Crystals by a Micro-pulling-down Method. *MRS Proc.* **2011**, *1309*, 33–38. [CrossRef]
25. Landau, L.D.; Lifchits, E.M. *Mecanique de Fluides*; Mir: Moscow, Russia, 1971; p. 132.
26. Balint, A.M.; Balint, S.; Tanasie, L. An axis symmetric 2D description of a single crystal micro fiber growth process from the melt by micro-pulling-down method. Part 1. *Math. Eng. Sci. Aerosp.* **2019**, *10*, 759–770.
27. Hartman, P. *Ordinary Differential Equations*; John Wiley & Sons: New York, NY, USA, 1964.
28. Balint, A.M.; Stefan, B. A 2D description of the single crystal thin plate growth from the melt by micro-Pulling-down method. Part 1. *INCAS Bull.* **2018**, *10*, 37–52. [CrossRef]
29. Balint, A.M.; Balint, S.; Tanasie, L. An axis symmetric 2D description of the growth process of a single crystal hollow tube, grown from the melt by pulling down method. Part. 1. *Math. Eng. Sci. Aerosp.* **2019**, *10*, 143–162.
30. Balint, A.M.; Balint, S. Existence and Stability of the Solution of a Nonlinear Boundary Value Problem. *Abstr. Appl. Anal.* **2012**, *2012*, 582746. [CrossRef]
31. Balint, A.M.; Stefan, B. Dynamics and control of the shape and size of a sitting drop like meniscus, occurring in single crystal growth. *J. Frankl. Inst.* **2010**, *347*, 30–52. [CrossRef]
32. Balint, A.M.; Balint, S.; Tanasie, L. An axis symmetric 2D description of a single crystal micro fiber growth process from the melt by micro-pulling-down method. Part 2. *Math. Eng. Sci. Aerosp.* **2019**, *10*, 771–780.
33. Balint, A.M.; Stefan, B. A 2D description of the single crystal thin plate growth from the melt by micro-Pulling-down method. Part 2. *INCAS Bull.* **2018**, *10*, 53–64. [CrossRef]
34. Balint, A.M.; Balint, S.; Tanasie, L. An axis symmetric 2D description of the growth process of a single crystal hollow tube, grown from the melt by pulling down method. Part. 2. *Math. Eng. Sci. Aerosp.* **2019**, *10*, 163–174.

Disclaimer/Publisher's Note: The statements, opinions and data contained in all publications are solely those of the individual author(s) and contributor(s) and not of MDPI and/or the editor(s). MDPI and/or the editor(s) disclaim responsibility for any injury to people or property resulting from any ideas, methods, instructions or products referred to in the content.